17p.

IN-34260

FINAL REPORT

For NASA Grant NAGW-200

May 15, 1981 - May 15, 1984

Studies of the Composition of Solar Particles and of Energetic Oxygen and Sulfur Nuclei Trapped in the Jovian Magnetosphere

(NASA-CR-179863) STUDIES OF THE COMPOSITION OF SOLAR PARTICLES AND OF ENERGETIC OXYGEN AND SULFUR NUCLEI TRAPPED IN THE JOVIAN MAGNETOSPHERE Final Report, 15 May 1981 - 15 May 1984 (California Inst. of Tech.) G3/91

N87-11672

Unclas 43962

Principal Investigator: E. C. Stone
California Institute of Technology
220-47 Downs Laboratory
Pasadena, CA 91125

The Cosmic Ray System (CRS) on the Voyager Spacecraft

The Cosmic Ray System (CRS) experiment on board each of the Voyager 1 and 2 spacecraft consists of four Low Energy Telescopes (LETs), two High Energy Telescopes (HETs), The Electron Telescope (TET), and associated electronics. With these instruments it is possible to measure the energy spectrum of electrons over the 3-110MeV energy range and the energy spectra and nuclear charge of atomic nuclei from hydrogen through zinc over the 3-500 MeV/nuc energy range. The exclusive use of solid-state detectors in the CRS telescopes achieves the objectives of reliability over a long mission life, high resolution determinations of energy and charge, and high-count-rate capability during large solar flares and passage through the magnetospheres of the outer planets. We summarize here some of the many accomplishments that have resulted from the CRS measurements during the period covered by this report, May 15, 1981 to May 15, 1984.

Studies of Solar Energetic Particles - Solar energetic particles (SEPs) represent a sample of material that can be used to determine directly the composition of the Sun. The four LET telescopes on each of the Voyager 1 and 2 spacecraft are ideally suited to determine the composition of solar flare nuclei because of their excellent resolution, large geometry factor, and low threshold (see Figures 1 and 2). Prior to this reporting period Cook, Stone, and Vogt, using four large solar flare events, performed the most extensive measurements to that time of the elemental composition for 15 elements in the 5 to 15 MeV/nuc energy range. They found that for the four events the average SEP abundances are similar to abundances in the solar wind and to coronal measurements but differ from the abundances in the photosphere, with a uniform depletion of those elements with a first ionization potential (FIP) greater than ~9 eV. They therefore suggested that SEPs originate in the corona. They also found that the abundances vary from flare to flare in a way that could be described as a monotonic, separable function of nuclear charge Z.

Breneman and Stone extended the work of Cook, Stone, and Vogt by including more flares (10) and by analyzing more elements (20). Using measured SEP ionic charge states for 8 elements from Luhn et al. and calculations of Shull and van Steenberg to interpolate for other elements, they found that the ionic charge-to-mass ratio (Q/M) is the principal organizing parameter for the fractionation of SEPs by acceleration and propagation processes and for flare-to-flare variability (Figure 3). Since individual flares exhibit a Q/M-dependent fractionation with respect to the average of all flares, there is also likely a residual Q/M-dependent fractionation of the average flare composition with respect to the corona.

Since the elements with low first ionization potential (FIP $<$ 9 eV) show no FIP-dependent fractionation, the correction factor was determined by comparing the average SEP abundances of these elements to photospheric spectroscopic abundances (Figure 4) as a function of Q/M. The correction function was derived by making a least-squares fit to the data of a power law in Q/M and that

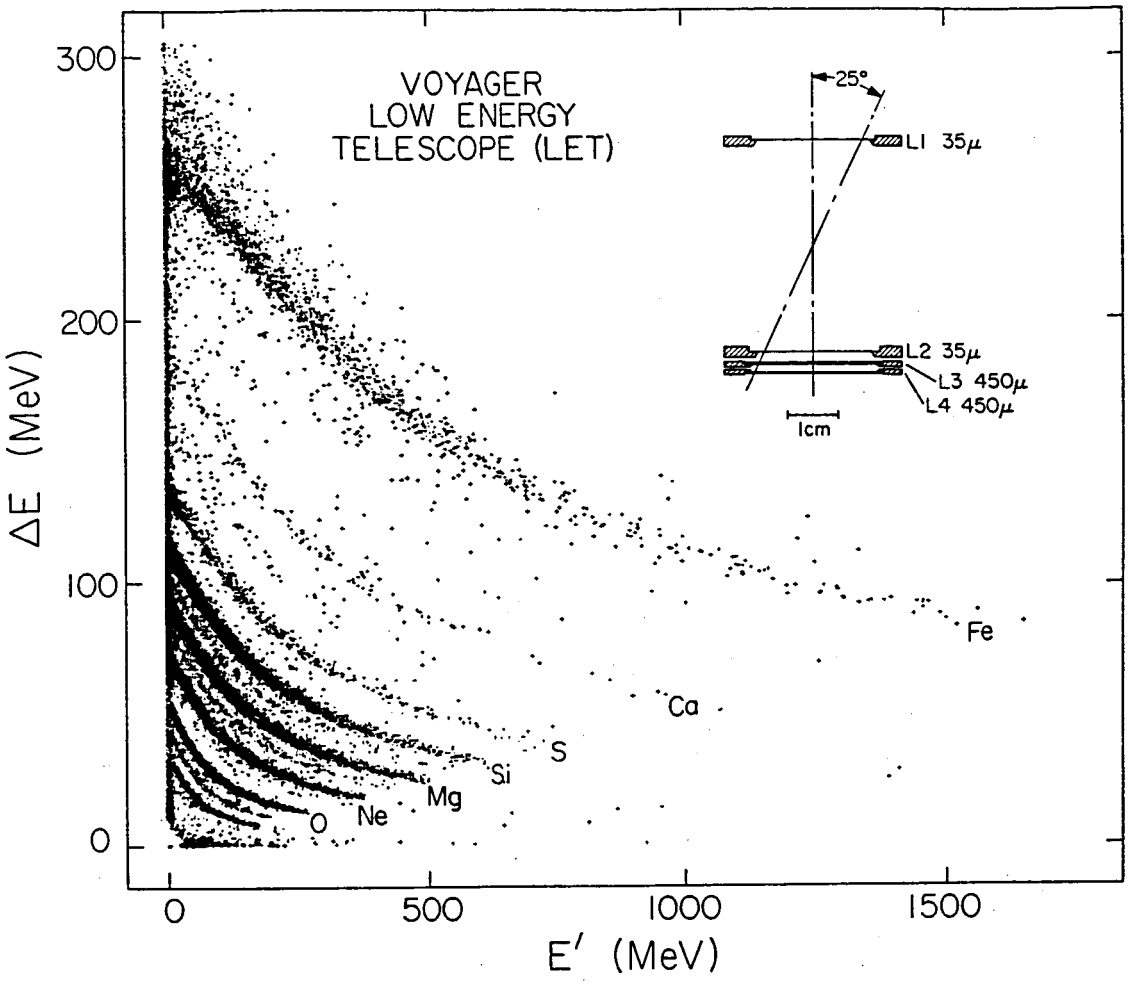

Fig. 1. LET schematic drawing and a scatter plot of raw flare data. The energy (ΔE) deposited in L1 is plotted vs. the sum (E') of energies deposited in detectors L2 and L3 for a sample of $Z \geq 3$ events from a LET on Voyager 1. (To prevent plot saturation, only every tenth event was plotted for elements oxygen and below.)

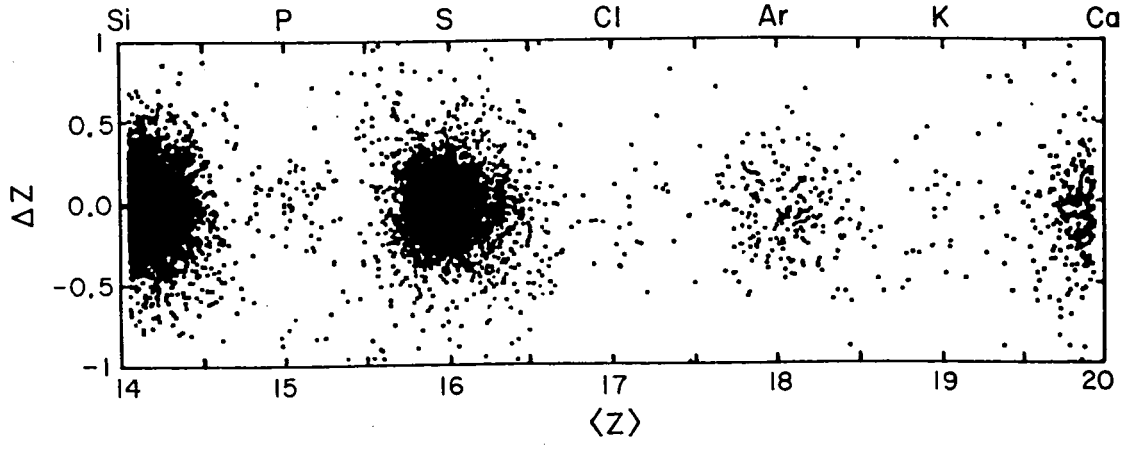

Fig. 2. Scatter plot of SEP data from LET in the Z = 14-20 charge range. $\langle Z \rangle$ is the average, and ΔZ is the difference, of two essentially independent charge determinations obtained from the LET data for each analyzed particle.

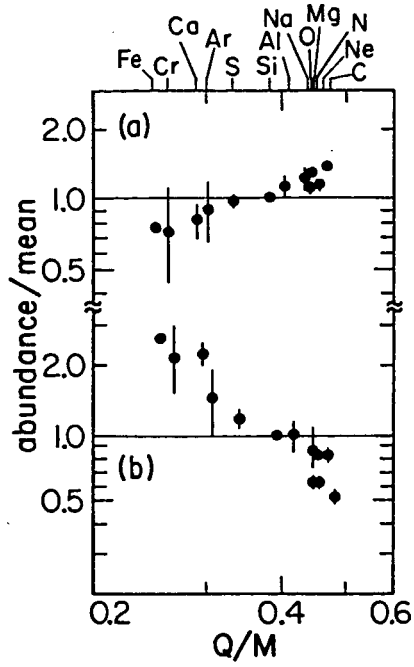

Fig. 3. Abundances relative to the mean SEP abundance for two typical flares, plotted vs. Q/M.

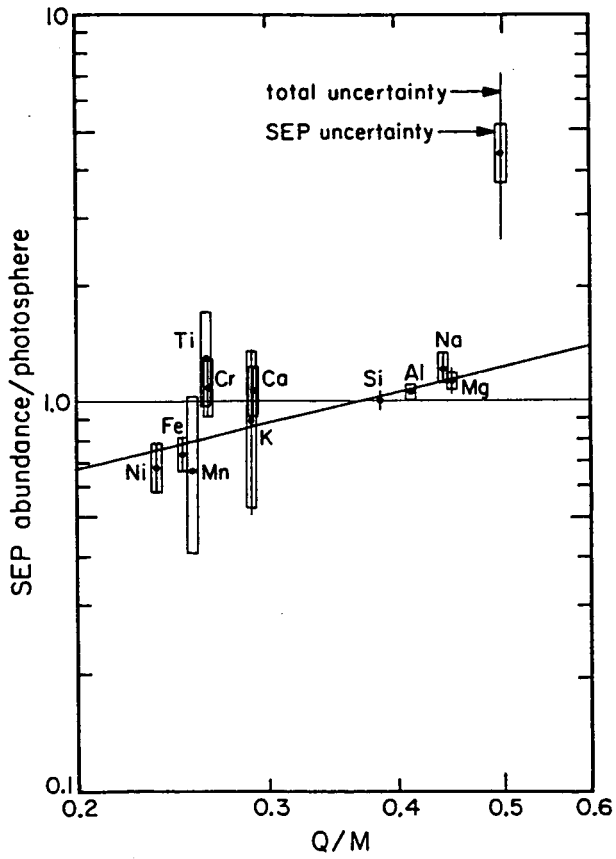

Fig. 4. Mean SEP abundance relative to the photosphere (Grevesse) for the low-FIP elements, plotted vs. Q/M. The fractionation of the SEP abundances relative to the photosphere is represented by a power law in Q/M which is fitted to all of the elements shown except Al, Ti, and Mn, which have unknown photospheric uncertainties.

correction was then applied to the SEP abundances for all elements, resulting in unfractionated SEP-derived coronal abundances. These abundances agree well with coronal abundances obtained by XUV/X-ray spectroscopy (Figure 5a), but have a much higher precision and are available for many more elements.

Breneman and Stone also compared the SEP-derived coronal abundances to the photospheric abundances (Figure 5b) and found that the step-function nature of the FIP-dependent fractionation was even more clearly defined than previously. They derived SEP photospheric abundances by applying a FIP correction based on Figure 5b. These SEP-derived abundances involve different modeling parameters than spectroscopic determinations and are available for some elements that are difficult or impossible to observe spectroscopically (e.g., C, N, Ne, Ar). The main differences (Figure 6) are a significantly higher abundance of Cr (and possibly Ca and Ti) and a C abundance that is about half of the commonly assumed solar value.

Energetic Oxygen and Sulfur in the Jovian Magnetosphere - Shortly after the Voyager 1 flyby of Jupiter the CRS team reported the discovery of energetic oxygen and sulfur (and some sodium) nuclei in the Jovian magnetosphere (see Figure 7). These particles originate on Io, thrown out from the moon in volcanic eruptions. Gehrels, Stone, and Trainor [1981] and Gehrels and Stone [1983] studied the behavior of these ions in the energy range 1-20 MeV/nuc and in the radial range 5-20 R_J to determine information about their acceleration and propagation processes.

Gehrels, Stone, and Trainor found that the Voyager 1 oxygen and sulfur fluxes inside ~18 R_J were the same as those of Voyager 2 to within a factor of 2. They were thus able to combine the measurements from both encounters to provide a more complete data set.

The sulfur and oxygen particles have initial energies of only eV/nuc near Io. The particles propagate by diffusion and are accelerated in some region to the 1-20 MeV/nuc energy range of the CRS LET telescopes. Since particle energies change in the diffusion process, the radial diffusion theory deals with particle phase space densities at constant first adiabatic invariant (or magnetic moment $M = p_\perp^2/2mB$ where m is the particle mass, B is the magnetic field strength, and $p_\perp$ is the momentum perpendicular to the B field direction) rather than three-dimensional space densities at constant energy. Gehrels, Stone, and Trainor calculated the phase-space densities of oxygen (Figure 8) and found that there is a steep positive radial gradient of the oxygen ions between 6 and 17 R_J. They postulated from their observations that plasma ions diffuse outward from the Io torus, are non-adiabatically accelerated in the outer magnetosphere (beyond 17 R_J), and then diffuse inward and outward from the acceleration region as energetic ions.

Gehrels and Stone extended the analysis by improving the radial resolution of the phase-space densities (Figure 9), by calculating the diffusive flow rates of both sulfur and oxygen ions, and by studying their possible contribution to the auroral activity on Jupiter.

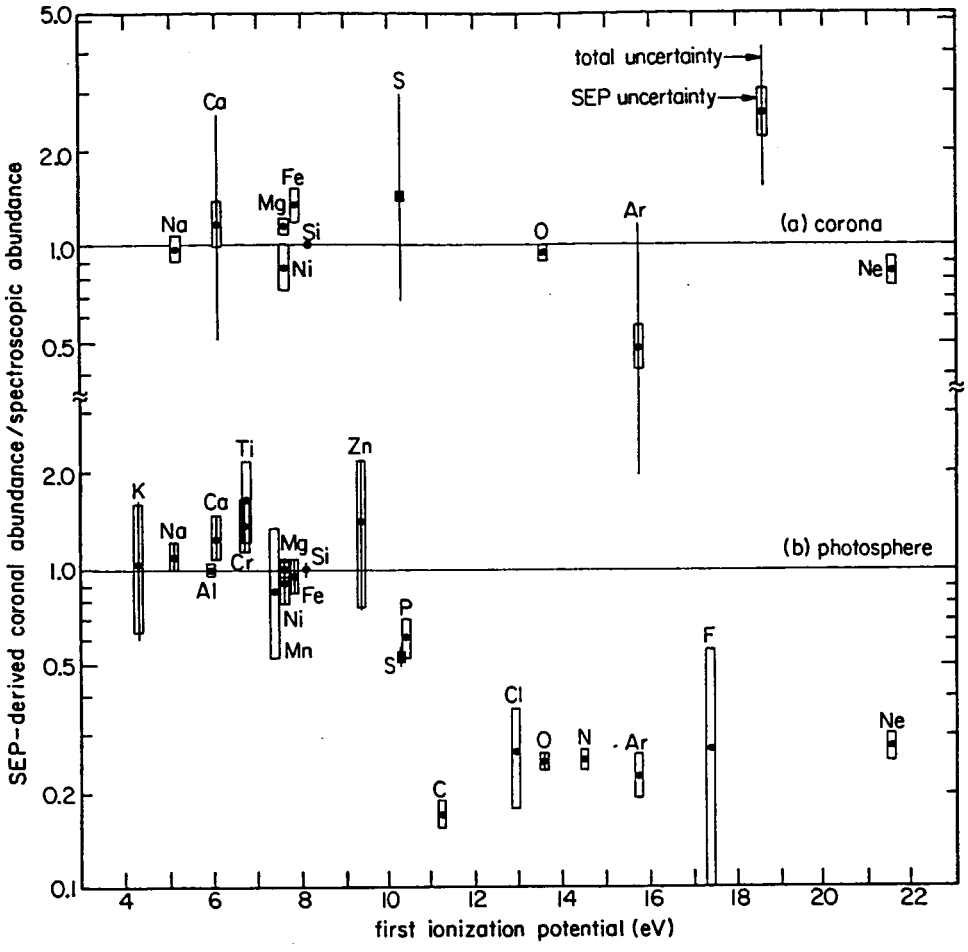

Fig. 5. (a) SEP-derived coronal abundances relative to spectroscopically derived coronal abundances (Veck and Parkinson), plotted vs. FIP. (b) SEP-derived coronal abundances relative to spectroscopic photospheric abundances (Grevesse), plotted vs. FIP.

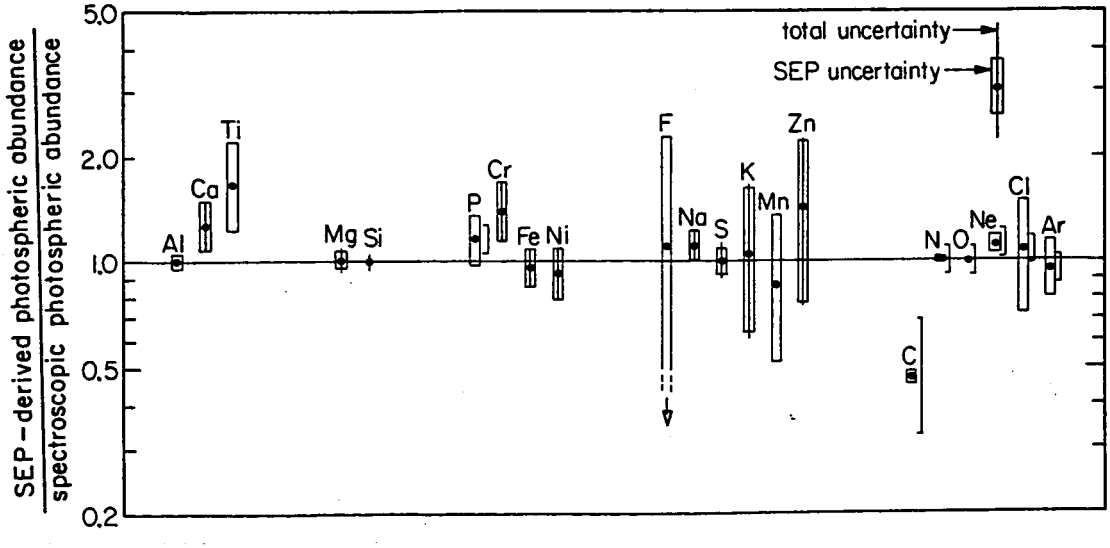

Fig. 6. SEP-derived photospheric abundances relative to spectroscopically derived photospheric abundances (Grevesse).

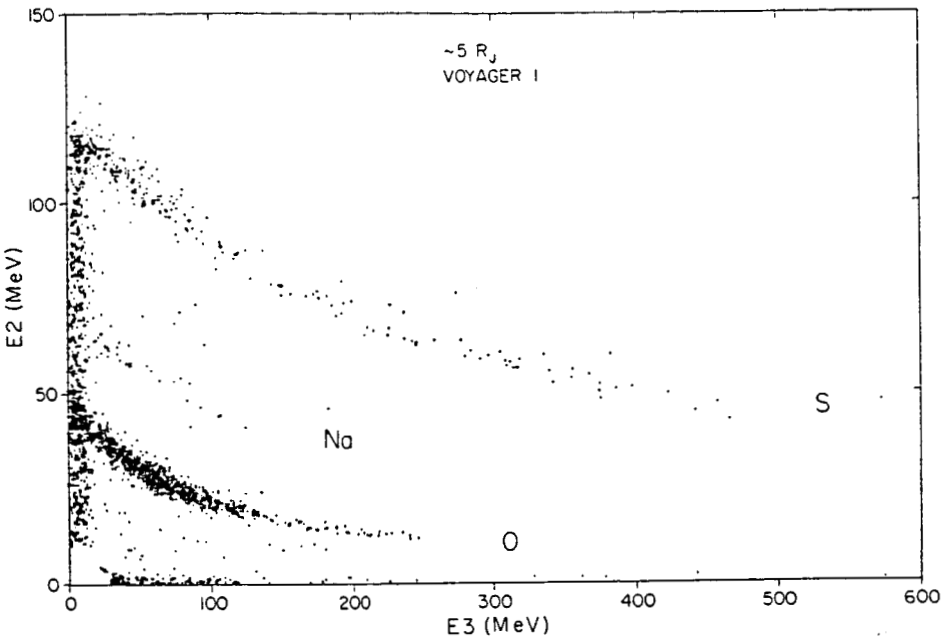

Fig. 7. The energy loss in detectors L2 and L3 of individual ions detected by LET D from day 64, 0936 to 1405 UT. The oxygen, sodium, and sulfur tracks are indicated. Events in the bottom left-hand corner have not been plotted.

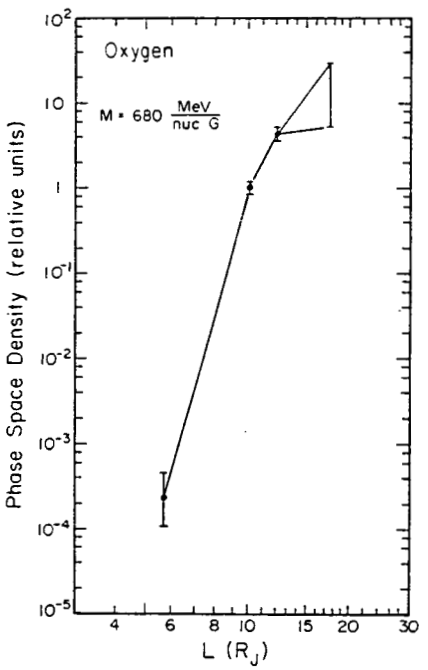

Fig. 8. The phase space density of oxygen ions with M = 680 MeV/nuc-G between L = 5.7 and L = 17.2. For L>12.1, f(L) was estimated by extrapolation of measurements at larger values of M. The uncertainty in this extrapolation is indicated by the error bar at L = 17.2.

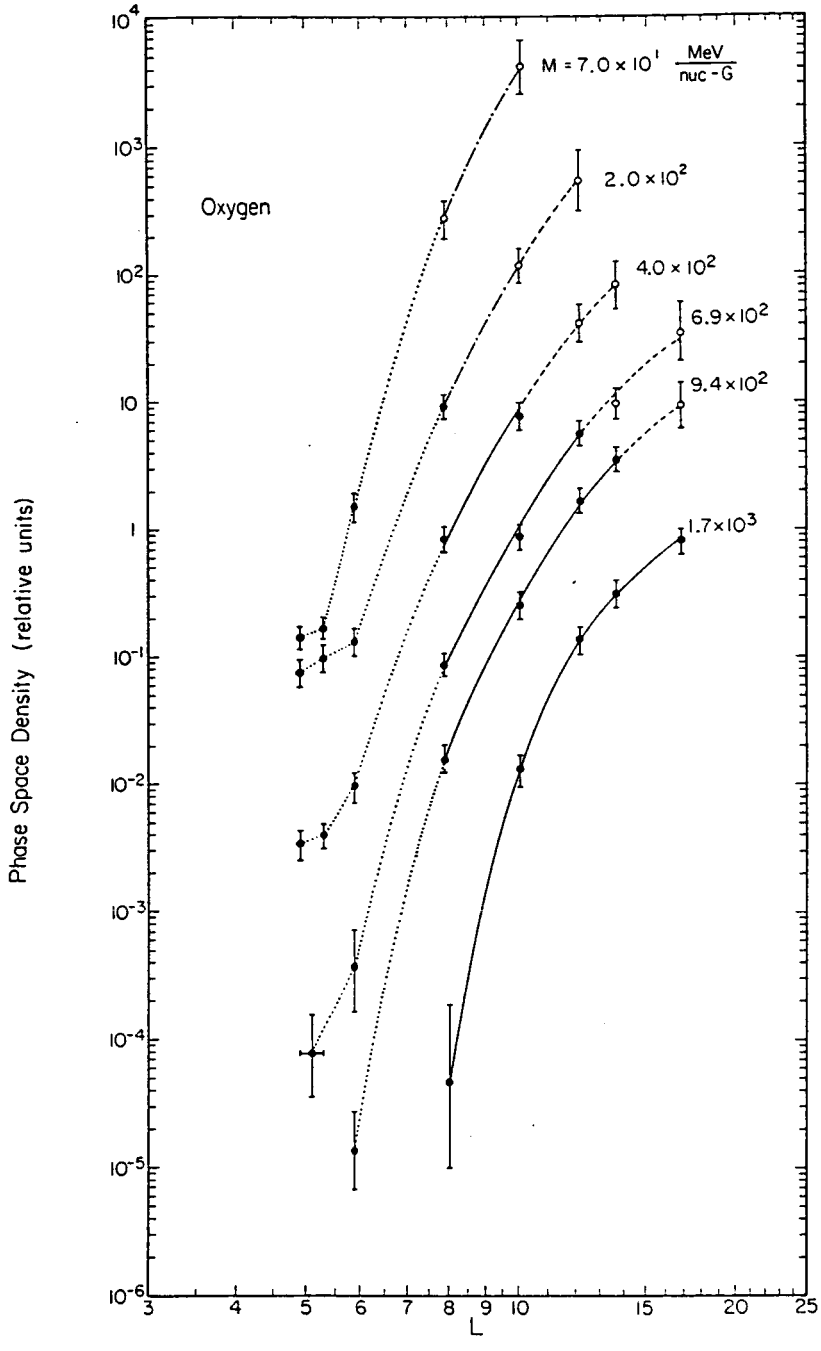

Fig. 9. The radial dependence of the phase space density of the energetic oxygen ions at constant magnetic moment, for several values of M. The solid points are derived from measured portions of the spectra, while the open points are based on extrapolations. Solid lines join the measurements at given magnetic moments between 7.9 and 16.9 R_J. The 5.3, 5.9, and 7.9 R_J measurements are connected by dotted lines to indicate that the radial profiles in this region may have discontinuities between the points.

They used the measured radial dependence of the oxygen phase space density in Figure 9 to obtain solutions to the diffusion equation and thereby set limits on the diffusion coefficient. They first considered the case of no losses between 6 and 17 R_J and found that the diffusion coefficient would have to have an index n ($D \propto L^n$) of less than -5 to fit the data. This would be inconsistent with other determinations of n using observations of energetic electrons and protons and of plasma in the region, which give $n = 4 \pm 2$. They concluded that there must be losses in the region and proceeded to consider the case of lossy diffusion.

The loss mode considered by Gehrels and Stone was that of strong pitch-angle scattering into the loss cone, i.e., particles scatter in pitch-angle such that they spiral into the atmosphere of Jupiter. They found that the upper limit to the diffusion coefficient at 9 R_J is $\sim 10^{-5}$/sec. This limit, combined with the analysis of Voyager plasma observations, specifies an upper limit to the mass loading rate near Io of $\sim 10^{28}$ ions/sec.

Their calculations showed that most of the energetic oxygen and sulfur ions are lost as they diffuse inward from 17 to 6 R_J, with the largest losses occurring between 12 and 8 R_J (Figure 10a). The oxygen and sulfur ions deposit most of their energy between $\sim 67°$ and $\sim 72°$ magnetic latitude (Figure 10b). This is consistent with the observed auroral zone width and is in the region where aurorae are seen. The vertical column depth in the Jovian atmosphere at which the bulk of the power is deposited is $\sim 10^{19}/cm^2$ of H_2, which is within the range of auroral depths derived from the observed wavelength dependence of ultraviolet emissions.

They also found that the amount of power delivered to the atmosphere by the energetic sulfur and oxygen ions is consistent with that required to produce the observed auroral emissions (Figure 11). Thus they suggested that energetic sulfur and oxygen ions from Io are responsible for the auroral activity on Jupiter, which is one of the most energetic phenomena associated with the Jovian magnetosphere.

Observations of Charged Particle Absorption Signatures in the Magnetosphere of Saturn - Two studies of energetic particles in Saturn's magnetosphere were also supported by grant NAGW-200. In the first, Chenette and Davis presented a new technique for determining the structure of Saturn's magnetic field by using the observed positions of charged particle absorption signatures due to satellites and rings of Saturn. They used absorption signatures observed along the Pioneer 11, Voyager 1, and Voyager 2 spacecraft trajectories to derive values for the orientation of the magnetic symmetry axis relative to Saturn's axis of rotation, the axial displacement of the center of the magnetic dipole from the center of Saturn, and the the magnitude of the external field component. By comparing their results with the magnetic field model parameters deduced from analyses of magnetometer data they find better agreement with the models which incorporate a northward offset of the dipole center by about 0.05 R_S (see Figure 12).

In the second study, Chenette and Stone analyzed the electron absorption signature observed by the CRS experiment on Voyager 2 near the orbit of Mimas

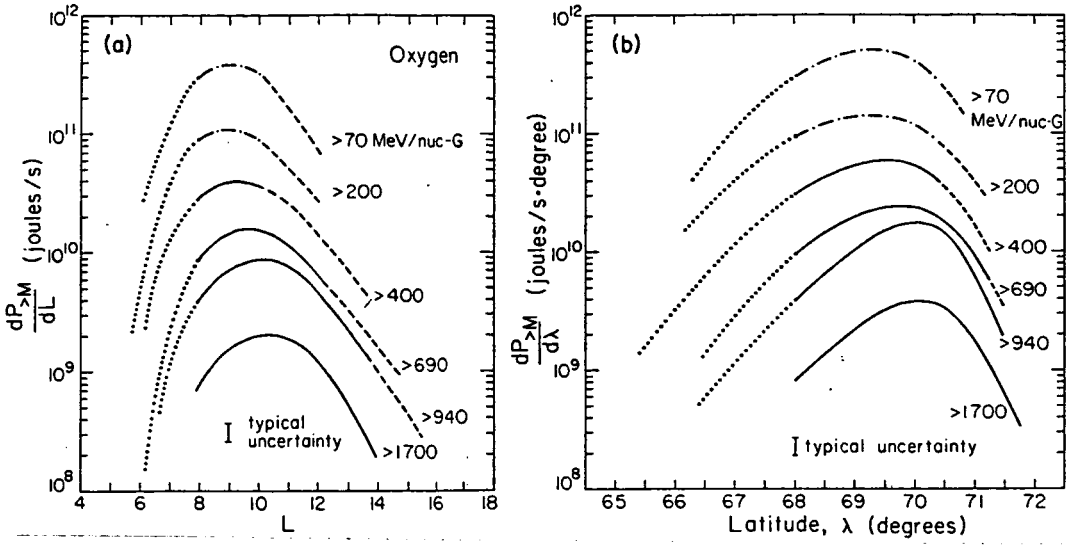

Fig. 10. The power delivered to the Jovian atmosphere (a) per unit L and (b) per degree magnetic latitude bu oxygen ions with magnetic moments greater than the indicated values. Typical error bars are shown.

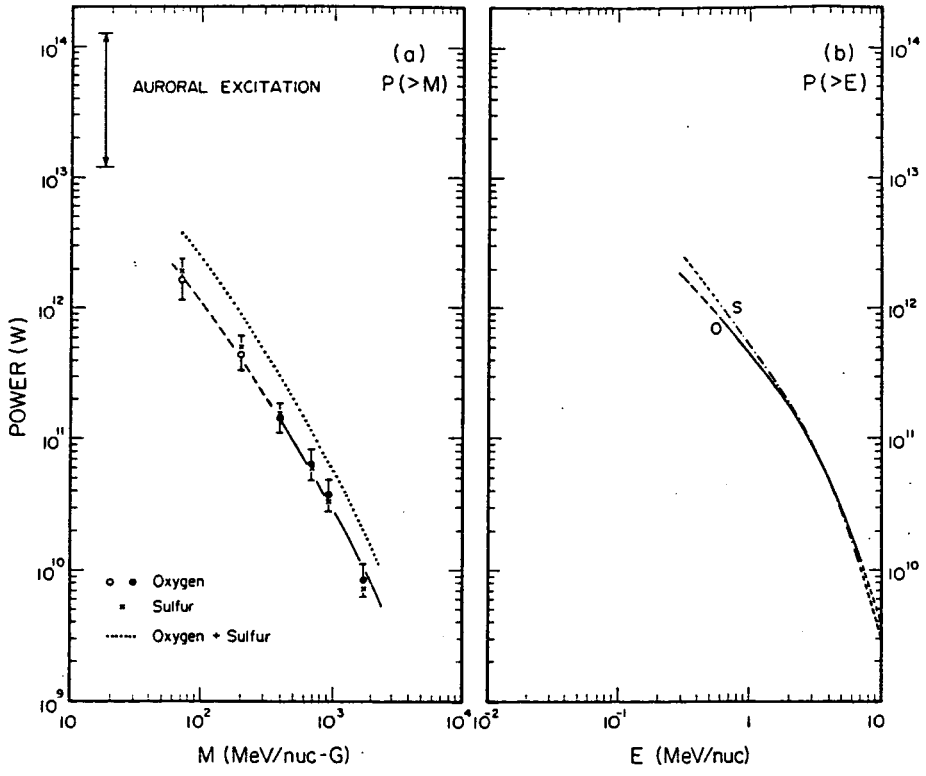

Fig. 11. The total power delivered by oxygen and sulfur ions (a) with magnetic moments greater than M and (b) energy greater than E to the Jovian atmosphere. The solid circles in (a) are based on measured portions of the spectra and the open circles are based on extrapolated portions. The range of estimates of the power required to excite the observed auroral activity (Broadfoot; Yung et al.) is also shown. In (b) the dashed portions indicate energies at which the calculation is based on extrapolations of the measured data.

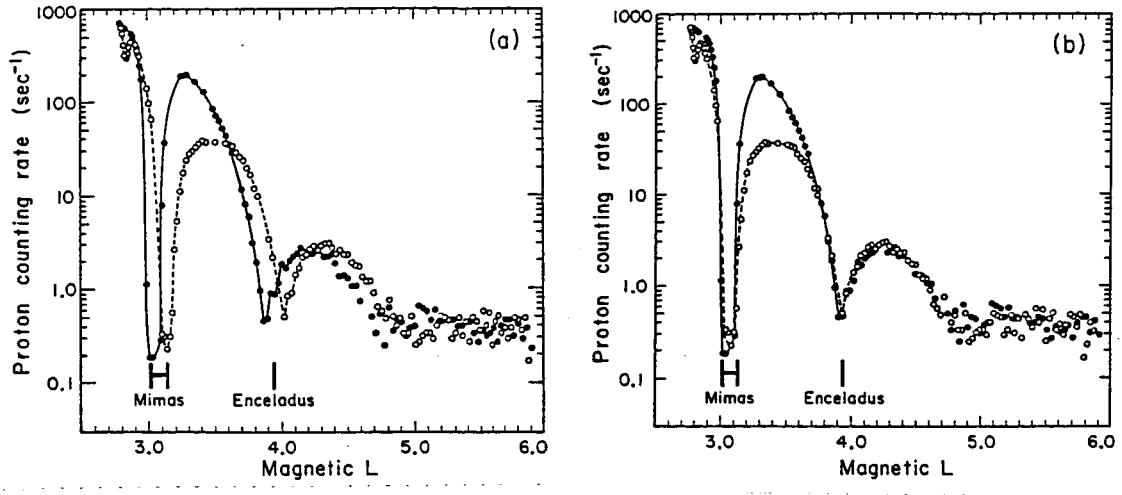

Fig. 12. The counting rate from the CRS on Voyager 2 which responds to protons in the energy range 63 - 160 MeV, plotted vs. L, for two different dipole magnetic field models. In part (a), the dipole was assumed to be centered on Saturn, while in part (b) the dipole was assumed to be offset north by 0.05 Saturn radii. In both cases the dipole was assumed to be aligned with Saturn's axis of rotation. Open symbols connected by dashed lines represent data obtained along the inbound pass. Filled symbols connected by solid lines represent data from the outbound pass. The positions of two of Saturn's inner satellites are indicated.

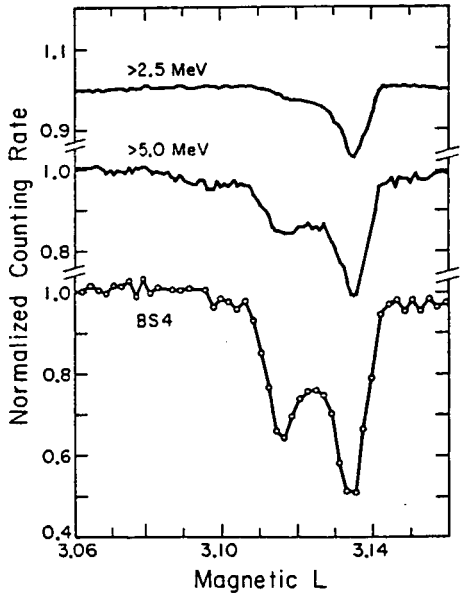

Fig. 13. A plot of the electron signatures near Mimas.

(Figure 13). They found that the observations could not be explained as the absorption signature of Mimas. Combining Pioneer 11 and Voyager 2 measurements of the electron flux at Mimas's orbit (L = 3.1), they found an electron spectrum where most of the flux above ~100 keV is concentrated near 1 to 3 MeV. This spectral form is qualitatively consistent with the band-pass filter model of Van Allen et al. The expected Mimas absorption signature was calculated from this spectrum neglecting radial diffusion. Since no Mimas absorption signature was observed in the inbound Voyager 2 data, a lower limit on the diffusion coefficient for MeV electrons at L = 3.1 of $D > 10^{-8} R_S^2/sec$ is obtained. With a diffusion coefficient this large, both the Voyager 2 and the Pioneer 11 small-scale electron absorption signature observations in Mimas's orbit are a mystery. Chenette and Stone estimated that a cloud of material in orbit with Mimas could account for the observed electron signature if the cloud is at least 1% opaque to electrons across a region extending over a few hundred kilometers.

Studies of the Anomalous Cosmic-Ray Component - The anomalous cosmic-ray (ACR) component consists of enhanced fluxes of He, N, O, and Ne with energies below ~50 MeV/nuc which are thought to be interstellar neutrals which drift into the heliosphere, become singly ionized, and are then convected to the outer heliosphere where they are accelerated. The Voyager CRS LET telescopes, with their large geometry factors and excellent resolution, are ideally suited to the study of this component. Several studies of this component on both short and long time scales were initiated under this grant.

The short-term study revealed several time periods where large periodic (typically 26 day) temporal variations of the ACR oxygen intensity between ~5-15 MeV/nuc were present, with variations in intensity by up to a factor of 10 (Figure 14). These variations are correlated with similar, but much smaller, variations in the >75 MeV/nuc nuclei rate. These intensity variations are apparently not high-energy extensions of low-energy increases associated with corotating interaction regions (CIR's), because the C/O ratio is much too small (0.05 compared to 0.7 in CIR's) and because the increases are out of phase with the CIR increases. It was also determined that the oxygen variations could not be explained as a local modulation effect because the local gradient as determined from a ratio of the Voyager 1 to the Voyager 2 intensities did not agree with the large-scale gradient. The origin of the variations thus remains unknown.

The study of the long-term behavior of the ACR oxygen revealed a very large variation in intensity by a factor of 300 or more from solar minimum levels in 1977-78 to solar maximum in 1980-81 (Figure 15). Despite the low ACR fluxes during the solar maximum period it was shown that the ACR component never completely "disappeared" and began to increase in intensity after the flux minimum in 1980-81.

The shapes of the energy spectra of ACR He, N, O, and Ne measured during solar minimum were compared and found to yield information on the charge state of the particles. In particular, the peak in the spectrum of ACR He is in the 10-20 MeV/nuc energy range (Figure 16), whereas the peak intensity of ACR O occurs at ~ 5 MeV/nuc. If the source spectra of these particles are similar

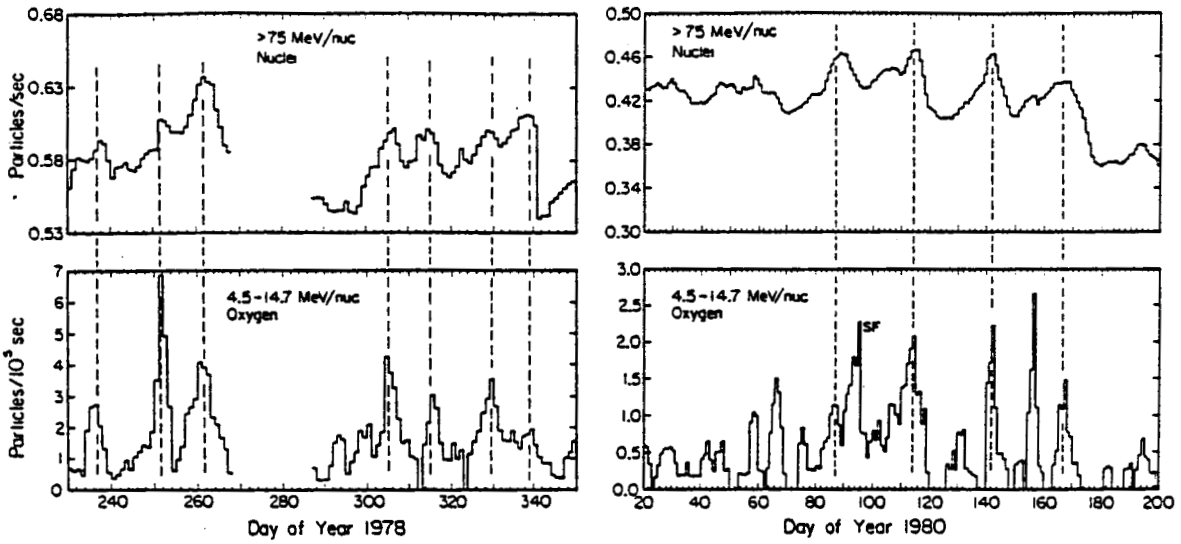

Fig. 14. Voyager 2 three-day moving average counting rate versus time for high-energy nuclei (upper panels) and anomalous O (lower panels) in 1978 (left) and 1980 (right). The dashed lines mark corresponding peaks in the two panels. Two 26-day sequences are indicated in 1978. Only one 26-day sequence is marked for 1980, although it is apparent that a weaker second series is present as well. The peak labeled SF is probably due to a solar flare. Note the offset in the vertical scale of the upper panels.

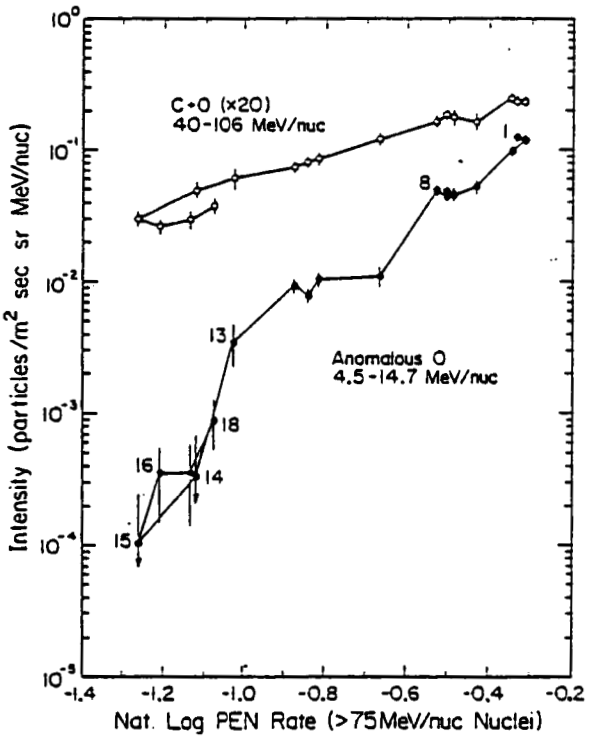

Fig. 15. Intensity of V1+V2 GCR C+O and anomalous O versus the PEN rate for 18 quiet-time intervals. The intensities have been corrected to 6 AU.

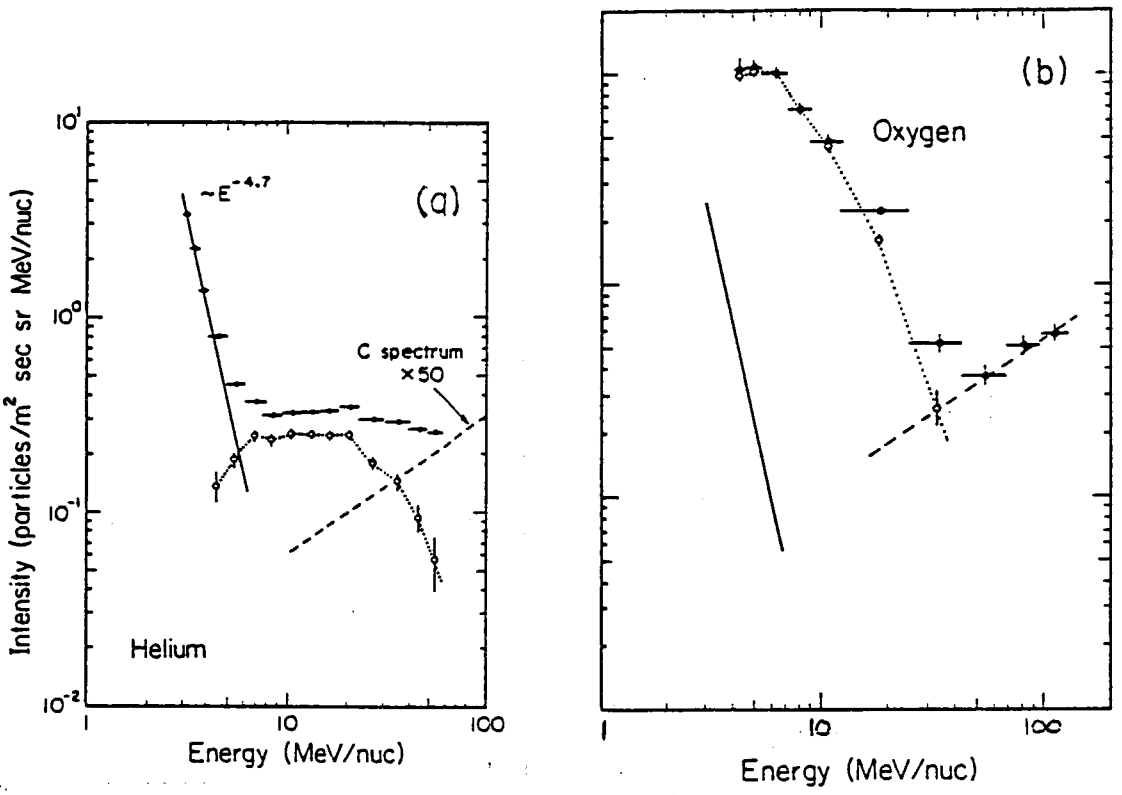

Fig. 16. (a) Composite V1+V2 quiet-time He spectrum for Sept. 1977 - Feb. 1978 time period. (b) Energy spectra of oxygen for same period. Quiet-time interplanetary component is shown as a solid line and estimated galactic component scaled from C is shown as the dashed line. Resulting anomalous component points (x's) are shown connected by the dotted line.

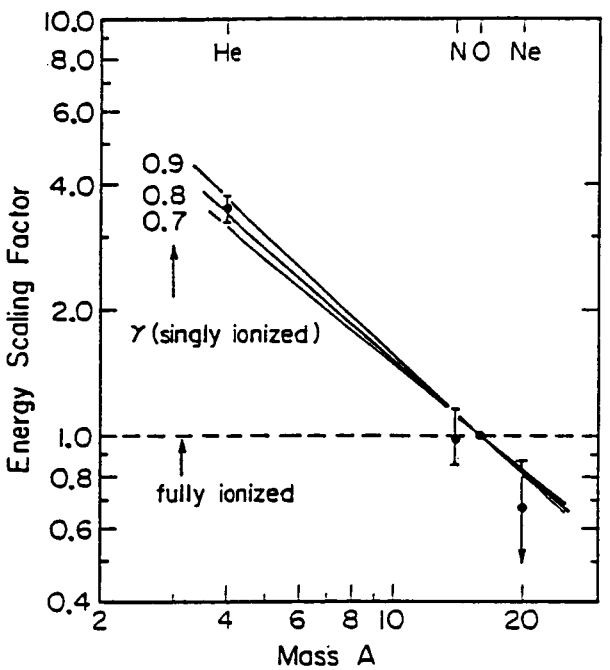

Fig. 17. Energy scaling factor f_E vs. mass A. The solid lines show the expected dependence on mass for singly ionized particles for 3 values of γ (in $\kappa \propto \beta R^{\gamma}$). The dashed line at $f_E = 1$ indicates the expected value for fully ionized particles with A/Z = 2.

then the location of the peak should occur at an energy for each species for which the particles have the same diffusion coefficient, κ. If $\kappa \propto \beta R^{\gamma}$, where R is rigidity and β is particle velocity, then the corresponding particle energies scale as $f_E(Z,A) \propto (A/Z)^{-2\gamma/(\gamma+1)}$. For fully ionized particles with $A/Z = 2$, the energy scaling factor f_E is independent of Z and the location of the peaks in the spectra should occur at the same value of energy/nucleon, as is observed for several galctic cosmic ray species such as C, O, Ne, Mg, and Si but not for the anomalous O and He. For singly-ionized particles ($Z = 1$), $f_E \propto A^{-2\gamma/(\gamma+1)}$ and the spectra should peak at different energies for particles with different A. The energy scaling factors were determined empirically by scaling the spectra of He, N, and Ne to the O spectrum (Figure 17). The observations are consistent with the particles being singly ionized and with $\kappa \propto \beta R^{0.8}$.

Bibliography for NASA Grant NAGW-200

"Energetic Oxygen and Sulfur in the Jovian Magnetosphere", N. Gehrels, E. C. Stone, and J. H. Trainor, JGR 86, 8906 (1981).

"An Analysis of the Structure of Saturn's Magnetic Field Using Charged Particle Absorption Signatures", D. L. Chenette and L. Davis, JGR 87, 5267 (1982).

"Energetic Oxygen and Sulfur Ions in the Jovian Magnetosphere", N. Gehrels, Ph.D. Thesis, California Institute of Technology, (1981).

"Energetic Oxygen and Sulfur in the Jovian Magnetosphere and Their Contribution to the Auroral Excitation", N. Gehrels and E. C. Stone, JGR 88, 5537 (1983).

"The Mimas Ghost Revisited: An Analysis of the Electron Flux and Electron Microsignatures Observed in the Vicinity of Mimas at Saturn", D. L. Chenette, and E. C. Stone, JGR 88, 8755 (1983).

"Temporal Variations of the Anomalous Oxygen Component", A. C. Cummings and W. R. Webber, Proc. Solar Wind V Conf., NASA CP 2280, 435 (1983).

"Voyager Measurements of the Energy Spectrum, Charge Composition, and Long Term Temporal Variations of the Anomalous Components in 1977-1982", W. R. Webber and A. C. Cummings, ibid 427, (1983).

"Studies of Low Energy Cosmic Rays - The Anomalous Component", W. R. Webber, A. C. Cummings, and E. C. Stone, 18th Int'l Cosmic Ray Conference, Bangalore, India, Conf. Papers (late paper).

"Short and Long Term Variations of the Anomalous Component", A. C. Cummings, R. A. Mewaldt, and W. R. Webber, ibid (late paper).

"Future Studies of Planetary Rings by Spaceprobes", E. C. Stone, A chapter in "Planetary Rings" Brahic and Greenberg, eds., U of AZ Press (in press 1984).

"The Saturn System", E. C. Stone and T. Owen, A chapter in "Saturn" Brahic and Greenberg, eds., U of AZ Press (in press 1984).

"Elemental Composition of Solar Energetic Particles", 18th Int'l Cosmic Ray Conference, Bangalore, India, Conf. Papers 4, 35 (1983).

"Energetic Oxygen and Sulfur Ions in the Jovian Magnetosphere and Their Contributions to the Auroral Excitation", N. Gehrels and E. C. Stone, 5th Conf. on the Physics of the Jovian and Saturnian Magnetospheres (1983).

"Solar Energetic Particle Abundances of Rare Elements", H. H. Breneman and E. C. Stone, Bull. Amer. Phys. Soc. (to be published 1984).

"Long and Short Term Variations of the Anomalous Component", A. C. Cummings, R. A. Mewaldt, and E. C. Stone, EOS Trans. 64, 791 (1983).

"Isotopic Composition of Solar Energetic Particles", S. P. Christon and E. C. Stone, ibid 64, 789 (1983).

"Rare Element Abundances in Solar Energetic Particles", H. H. Breneman and E. C. Stone, ibid 64, 789 (1983).

"Diffuse Aurora at Jupiter", E. C. Stone, ibid 64, 804 (1983).

The Cosmic Ray System (CRS) on the Voyager Spacecraft

The Cosmic Ray System (CRS) experiment on board each of the Voyager 1 and 2 spacecraft consists of four Low Energy Telescopes (LETs), two High Energy Telescopes (HETs), The Electron Telescope (TET), and associated electronics. With these instruments it is possible to measure the energy spectrum of electrons over the 3-110 MeV energy range and the energy spectra and nuclear charge of atomic nuclei from hydrogen through zinc over the 3-500 MeV/nuc energy range. The exclusive use of solid-state detectors in the CRS telescopes achieves the objectives of reliability over a long mission life, high resolution determinations of energy and charge, and high-count-rate capability during large solar flares and passage through the magnetospheres of the outer planets. We summarize here some of the many accomplishments that have resulted from the CRS measurements during the period covered by this report, May 15, 1981 to May 15, 1984.

Studies of Solar Energetic Particles - Solar energetic particles (SEPs) represent a sample of material that can be used to determine directly the composition of the Sun. The four LET telescopes on each of the Voyager 1 and 2 spacecraft are ideally suited to determine the composition of solar flare nuclei because of their excellent resolution, large geometry factor, and low threshold (see Figures 1 and 2). Prior to this reporting period Cook, Stone, and Vogt, using four large solar flare events, performed the most extensive measurements to that time of the elemental composition for 15 elements in the 5 to 15 MeV/nuc energy range. They found that for the four events the average SEP abundances are similar to abundances in the solar wind and to coronal measurements but differ from the abundances in the photosphere, with a uniform depletion of those elements with a first ionization potential (FIP) greater than ~9 eV. They therefore suggested that SEPs originate in the corona. They also found that the abundances vary from flare to flare in a way that could be described as a monotonic, separable function of nuclear charge Z.

Breneman and Stone extended the work of Cook, Stone, and Vogt by including more flares (10) and by analyzing more elements (20). Using measured SEP ionic charge states for 8 elements from Luhn et al. and calculations of Shull and van Steenberg to interpolate for other elements, they found that the ionic charge-to-mass ratio (Q/M) is the principal organizing parameter for the fractionation of SEPs by acceleration and propagation processes and for flare-to-flare variability (Figure 3). Since individual flares exhibit a Q/M-dependent fractionation with respect to the average of all flares, there is also likely a residual Q/M-dependent fractionation of the average flare composition with respect to the corona.

Since the elements with low first ionization potential (FIP $<$ 9 eV) show no FIP-dependent fractionation, the correction factor was determined by comparing the average SEP abundances of these elements to photospheric spectroscopic abundances (Figure 4) as a function of Q/M. The correction function was derived by making a least-squares fit to the data of a power law in Q/M and that